Algorithm to Calculate Frictional Power Loss Between Bodies During Rotation Under Contact Stress

Slavomír Hrček[1](✉), Michal Lukáč[1], and Ján Šteininger[2]

[1] University of Žilina, Univerzitná 8215/1, 010 26 Žilina, Slovakia
slavomir.hrcek@fstroj.uniza.sk

[2] Institute of Competitiveness and Innovations, Univerzitná 8215/1, 010 26 Žilina, Slovakia

Abstract. The article deals with the proposed algorithm for calculating the frictional power loss generated by the influence of sliding in bodies during their rotation under contact stress. PTC/Creo Parametric CAD system was used for creation of parametric 3D virtual model of rolling bearings due to FEM analysis. For FEM analysis, the static structural analysis for rolling bearing model was defined in Ansys/Workbench CAE software. Dimensions of bearing are: pitch diameter: $dpw = 548$ mm, roller diameter: $dwe = 41.7$ mm, roller length: $lwe = 61.2$ mm, nominal contact angle: $\alpha 0 = 28°$, revolution of inner ring: $ni = 25$ rpm, radial load: $Q\max = 255$ kN. For all rolling bearing components a linear isotropic elasticity material model with Young's modulus $E = 210$ GPa and Poisson's ratio $\mu = 0.3$ for bearing steels were use. The results will be presented on the example of a rolling bearing with spherical and taper shapes of rolling elements.

Keywords: Frictional Power Loss · Friction · Algorithm · Roller Bearings

1 Introduction

It is universally recognized that friction due to rolling of nonlubricated surfaces over each other is considerably less than the dry friction encountered by sliding the identical surfaces over each other. Notwithstanding the motions of the contacting elements in rolling bearings are more complex than is indicated by pure rolling, rolling bearings exhibit considerably less friction than most fluid film or sleeve bearings of comparable size and load-carrying ability [1].

Friction of any magnitude represents an energy loss and causes a retardation of motion. Hence friction in a rolling bearing is witnessed as a temperature increase and may be measured as a retarding torque [1].

The sources of friction in rolling bearings are manifold, the principal sources being as follows: elastic hysteresis in rolling, sliding between bearing components, viscous drag of the lubricant on the rolling elements and cage, seal friction [1].

This paper will deal with the calculation of frictional power loss generated at the raceways between the rolling elements and the bearing rings and between roller ends and ring flanges. The aim of the study was calculate frictional power loss between bodies during rotation under contact stress.

J. Homišin et al. (Eds.): ICMD 2020, AHE 17, pp. 203–214, 2023.
https://doi.org/10.2991/978-94-6463-182-1_22

2 Materials and Methods

2.1 Hydrodynamic Lubrication

Because it appeared possible that lubricant films of significant proportions do occur in the contact zones between rolling elements and raceways under certain conditions of load and speed, several investigators have examined the hydrodynamic action of lubricants on rolling bearings according to classical hydrodynamic theory. Martin presented a solution for rigid rolling cylinders as early as 1916. In 1959, Osterle considered the hydrodynamic lubrication of a roller bearing assembly [1].

Main problem in hydrodynamic lubrication is to model the pressure in a lubricant (fluid) between two surfaces which are in relative motion. Consideration of the full film.

regime, i.e. when the surfaces are fully separated by the lubricant was analyzed in. However, in real applications the distance between the surfaces is extremely small in relation to the size of the surfaces [2].

It is of interest at this stage to examine the mechanism of hydrodynamic lubrication at least in two dimensions. Accordingly, consider an infinitely long roller rolling on an infinite plane and lubricated by an incompressible isoviscous Newtonian fluid viscosity η. For a Newtonial fluid, the shear stress τ at any point obeys the relationship [1].

$$\tau = \eta \frac{\partial u}{\partial z} \tag{1}$$

in which ∂u/∂z is the local fluid velocity gradient in the z direction (see Fig. 1, left). Because the fluid is viscous, fluid inertia forces are small compared to the viscous fluid forces.

Hence a particle of fluid is subjected only to fluid pressure and shear stresses as shown in Fig. 1 (right).

Noting the stresses of Fig. 1 (right) and recognizing that static equilibrium exists, the sum of the forces in any direction must equal zero. Therefore

$$pdz - \left(p + \frac{\partial p}{\partial y}\right)dz + \tau dy - \left(\tau + \frac{\partial \tau}{\partial z}\right)dy = 0; \; and \; \frac{\partial p}{\partial y} = -\frac{\partial \tau}{\partial z} \tag{2}$$

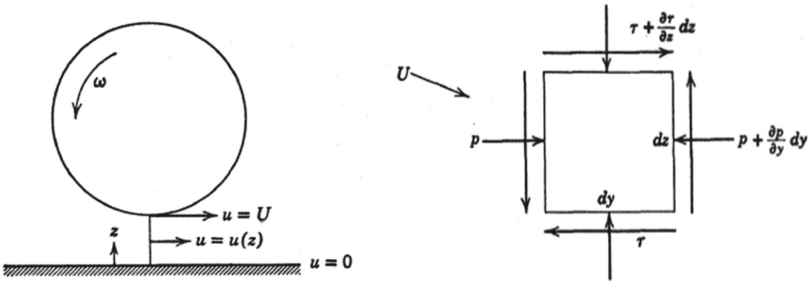

Fig. 1. Cylinder rolling on a plane with lubricant between cylinder and plane (left) [1]. Stresses on a fluid particle in a two-dimensional flow field (right) [1].

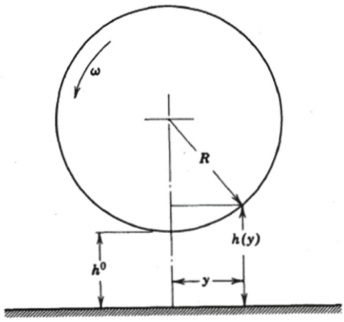

Fig. 2. Film thickness *h(y)* in the contact between a roller and plane [1].

After integrating Eq. 2 with respect to z

$$\frac{\partial}{\partial y}\left(h^2\frac{\partial p}{\partial y}\right) = 6\eta U\frac{\partial h}{\partial y} \tag{3}$$

Equation 3 is commonly called the Reynolds equation in two dimensions [1].

2.2 Film Thickness

To solve the Reynolds equation [1, 3] it is only necessary to evaluate film thickness as a function of y, that is, $h = h(y)$. For a cylindrical roller near a plane as shown by Fig. 2, it can be seen that

$$\frac{\partial}{\partial y}\left[h^0 + \left(\frac{y^3}{2R}\right)^3\frac{\partial p}{\partial y}\right] = \frac{6\eta U y}{R} \tag{4}$$

in which h^0 is the minimum film thickness [1].

2.3 Pressure and Stress Distribution

According to [1], in a later presentation Dowson (Eq. 4) indicated that dimensionless film thickness $H = h/\Re$ could be expressed as follows

$$H = f\left(\overline{Q}, \overline{U}, G\right) \tag{5}$$

$$\overline{Q} = \frac{Q_z}{lE'\Re} \tag{6}$$

$$\overline{U} = \frac{\eta_0 U}{2E'\Re} \tag{7}$$

$$E' = \frac{\mathrm{E}}{1-\nu^2} \tag{8}$$

where Q_z is a force acting on roller, l is a roller effective length, E is a modulus of elasticity, $\Re$ is an equivalent radius, η_0 is a dynamic viscosity, U is an entrance velocity of oil. Based upon analytical studies and experimental results as is mentioned in [1], Dowson established the following formula to calculate the minimum film thickness in line contact:

$$\overline{U} = \frac{2.65\overline{U}^{0.7}\}^{0.54}}{\overline{Q}^{0.13}} \tag{9}$$

where

$$\} = \lambda E' \tag{10}$$

λ is a pressure coefficient of viscosity.

Finally, minimum lubricant film thickness can be calculated,

$$h = H\Re \tag{11}$$

2.4 Viscosity Variation with Pressure

In 1893, Barus established an empirical equation to describe the variation of viscosity with pressure for a given liquid at a given temperature an isothermal relationship. Barus's equation is usually stated as follow, [1]:

$$\eta = \eta_0 e^{\lambda p} \tag{12}$$

Roelands later established an equation defining the viscosity-pressure relationship for given fluids, but including the influence of temperature on viscosity as well

$$\frac{log_{10}\eta + 1.2}{log_{10}\eta_0 + 1.2} = \left(\frac{T_0 + 135}{T + 135}\right)^{S_0}\left(1 + \frac{p}{2000}\right)^{z} \tag{13}$$

In Eq. 13, pressure (p) is expressed in kgf/cm^2 and temperature T in $°K$; exponents So and z are determined empirically for each lubricant. At high pressures, Eq. 13 indicates viscosities substantially lower than those produced using the Barus Eq. 12, see [1].

2.5 Contact Friction Force

Harris used 37 sets of data of traction coefficient *vs* slide-to-roll ratio and Λ collected on a *v*-ring-single ball test rig to generate the following empirical relationship:

$$\mu = -2.066x10^{-3} + 2.612x10^{-6}\left[\frac{1}{\Lambda} ln\left(\frac{\eta}{\eta_0}\right)\right]^2 - 5.605x10^{-2}\left[\frac{\nu}{U} ln\left(\frac{\nu}{U}\right)\right] \tag{14}$$

where η is the lubricant viscosity at contact pressure, η_0 is the lubricant viscosity at atmospheric pressure, and U is the rolling velocity [1]. Traction coefficient μ is directional. It might, however, be considered as occurring at a point in a contact such that τ_y

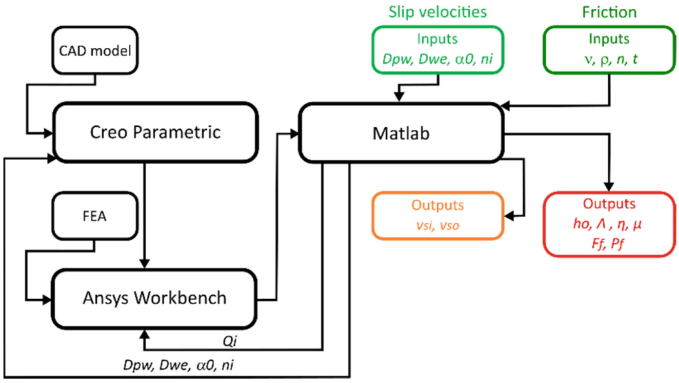

Fig. 3. Algorithm to calculate frictional power loss.

$= \mu_y \sigma$ and $\tau_x = \mu_x \sigma$. The lubricant used during the v-ring-ball testing was a Mil-L-236 99 polyolester [1].

Friction force, according to [1], F_f is calculated as conjunction of the normal force F_n and coefficient of friction μ calculated at each point along the line contact.

The instantaneous frictional power loss is according to [1], calculated as conjunction of the slip velocity v_s and the friction force F_f acting in the same direction

$$P_f = v_s * F_f \tag{15}$$

2.6 Proposal of Algorithm for Calculation Frictional Power Loss

The using of many advanced software tools is needed for calculation of sliding velocity in rolling bearings. The loading determines real deformation and then the real rolling radii include these deformations. The proper FEA software need to be used for determination. The inner geometry of rolling bearing is too complicated. Therefore, a useful CAD tool is recommended to use. Via this CAD tool should be possible also work with parametric model [5]. The FEA analysis results and mathematical calculations have to be evaluated. We used origin script for results evaluation, which one has been created in useful programming language. The Fig. 3 shows the algorithm for calculation of the frictional power loss in rolling bearings.

2.7 Virtual Model of Spherical Rolling Bearings

For FEM analysis, a fully parametric 3D virtual model of spherical or tapered rolling bearings was created in the PTC/Creo Parametric CAD system. These models were designed so that its geometry was controlled by the parameters through relations. In this way we were able to efficiently modify individual dimensions and create size-based series of spherical or tapered rolling bearings. The Fig. 4 shows a view with the control parameters.

2.8 FEM Analysis

In order to perform FEM analysis, we used Ansys/Workbench CAE software, in which we defined static structural analysis for the spherical or tapered rolling bearing model. The resulting virtual 3D model of a spherical or tapered rolling bearing was imported from the PTC/Creo Parametric system via an interface to the Ansys/Workbench environment. This interface enables us to modify the parameters and thus change the rolling bearing model directly from the Ansys/Workbench environment.

For all rolling bearing components we used a linear isotropic elasticity material model with Young's modulus $E = 210$ GPa and Poisson's ratio $\mu = 0.3$ for bearing steels [4]. We chose a linear material model because we applied such maximum normal load F_n acting on the rolling bearing with line contact that we would avoid exceeding the yield strength of the material and the maximum contact pressure exceeding $p_o = 3500$ MPa, which is defined as the threshold value for line contact.

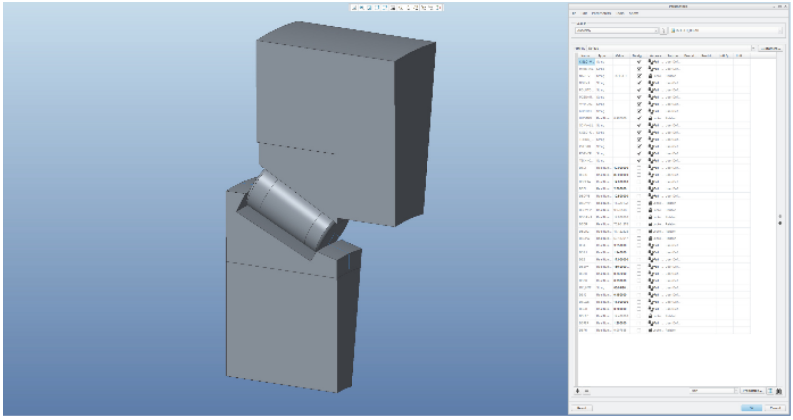

Fig. 4. Virtual model of tapered rolling bearings.

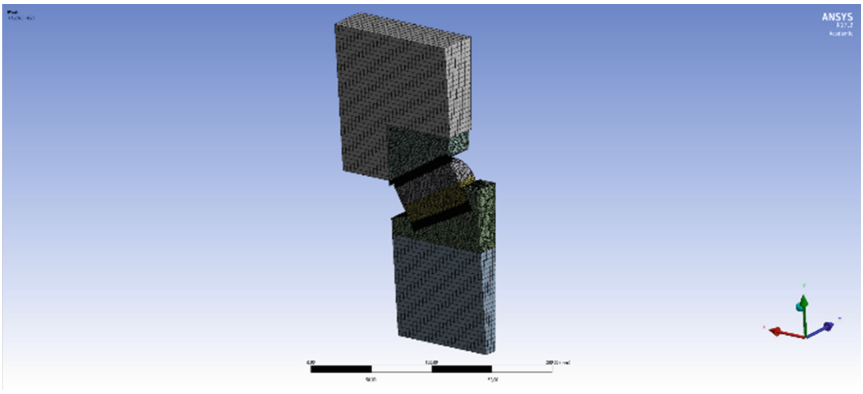

Fig. 5. FEM model of spherical rolling bearings.

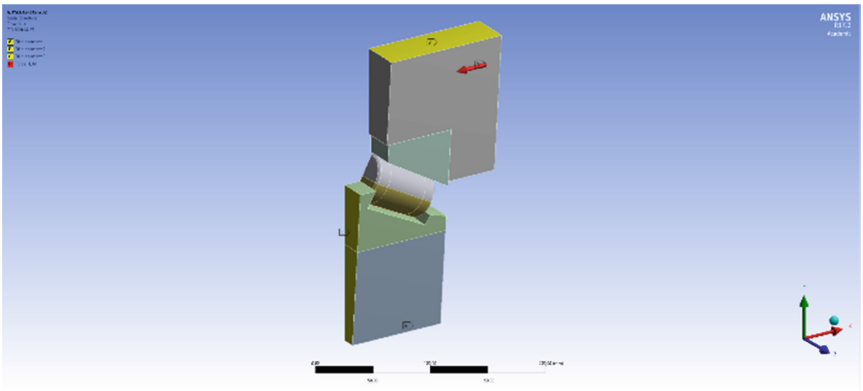

Fig. 6. Boundary conditions and load applied on FEA model TRB.

Symmetry was applied to the model in one plane X-Y for reducing the computational time. The model mesh (see Fig. 5) was created by standard elements from the Ansys library. The volume mesh was created with the SOLID185 element. Individual bearing elements are in contact because the forces acting upon the bearing are transferred between rings (their raceways) and roller. Elements type CONTA174 and TARGE170 were used for mesh contact pairs (rolling elements – raceways). Choosing an appropriate mesh element size is necessary in order to correctly analyze the contact pressure between the roller and raceway of the outer and inner rings.

The contacts between the rolling elements and orbital paths of the two rings (races) were defined as Frictionless type. The same type of contact was defined between the roller and ring flange.

The loading in axial direction is applied on housing. The boundary condition – displacement in X-axis is defined opposite of the axial load force on shaft and inner ring (see Fig. 6). The result of FEM analysis is the distribution of contact pressure and the deformations of raceway and ring flange of bearing rings and roller in contact area.

2.9 Processing Results from FEM Analysis

The deformations, which are evaluated by Ansys are not the true deformation. In this case we are talking about complex movement of nodes/elements. This complex movement includes body movement (e.g. due to close gap) and contact stiffness and true deformation. This is the reason why the subsequently evaluation of these results is still needed for determination of the true deformation. The origin script in Matlab was created for results evaluation. Output of this script is calculation of the true deformation of raceways for inner and outer rings and roller.

3 Results

Sliding velocities between the rolling element and the raceways are calculated from the true rolling radii and angular velocities at the points with pure rolling without slip. To calculate the angular velocities, the relationships for calculating the planetary gear can

be used, where the inner ring corresponds to a sun gear, the outer ring corresponds to the ring gear, the carrier is the cage and the satellites are rolling elements.

The proposed algorithm was used to calculate sliding velocities between the raceways and the rolling element shown in Fig. 7. Dimensions of bearing are: pitch diameter: $dpw = 548$ mm, roller diameter: $dwe = 41.7$ mm, roller length: $lwe = 61.2$ mm, nominal contact angle: $\alpha 0 = 28°$, revolution of inner ring: $ni = 25$ rpm, radial load: $Qmax = 255$ kN.

The Fig. 8 shows the calculated distribution of the partial normal (blue) and frictional (red) forces along the line contact at high bearing load.

The Fig. 9 shows the trend of the calculated coefficients of friction between the roller and the raceways and the ring flange. At low speeds with increasing load, the friction coefficient increases to a value close to 0.3, which already represents a steel-steel contact without lubricant.

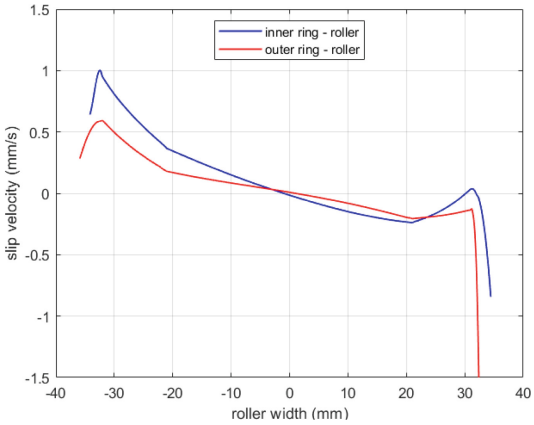

Fig. 7. Calculated sliding velocities for a TRB bearing at the given load.

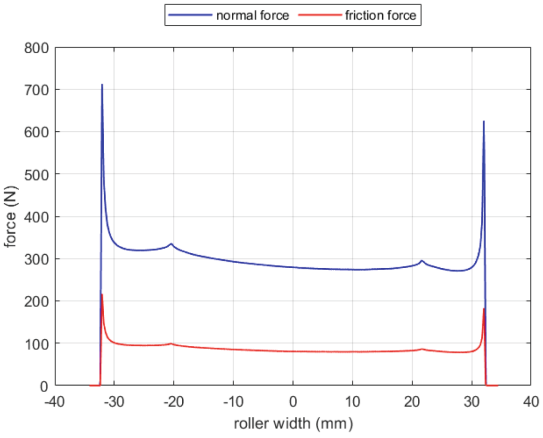

Fig. 8. Calculated normal and frictional force along roller width on inner ring.

The Fig. 10 shows the distribution of the contact pressure between the roller and the ring flange at high bearing load. The position of this zone relative to the position of the slip velocities (see Fig. 11) on the ring flange is very important to calculate frictional power loss.

The Fig. 12 shows the dependence of the calculated magnitude of the coefficient of friction between the roller and the ring flange on the magnitude of the slip velocity in the contact zone where the contact pressure acts.

The Fig. 13 shows the dependence of the power loss on the magnitude of the load between the main friction surfaces in the TRB. Low value of frictional less power on raceways is generated considering to low slip speeds. In the opposite, the largest frictional

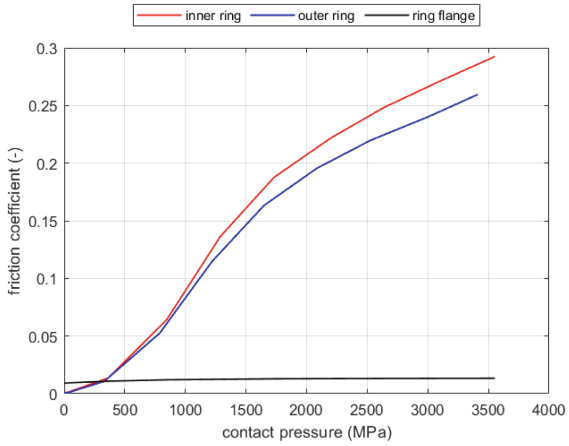

Fig. 9. Calculated frictional coefficients depend on contact pressure.

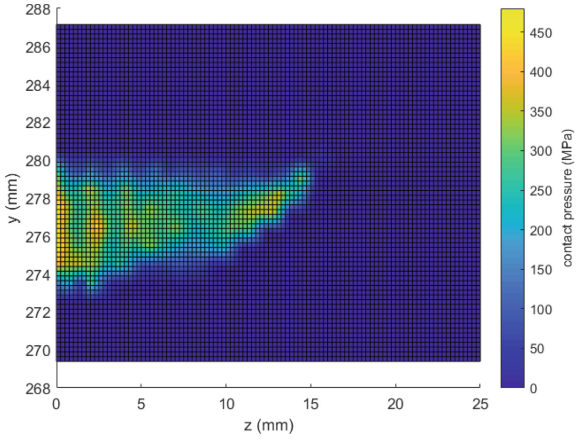

Fig. 10. Distribution of contact pressure on the contact surface of ring flange of tapered roller bearing.

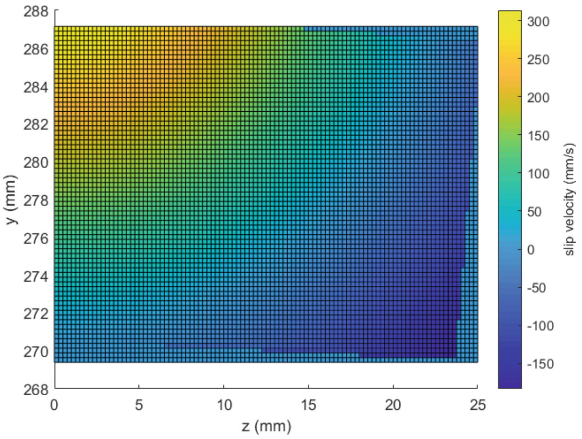

Fig. 11. Distribution of slip velocity on the contact surface of ring flange of tapered roller bearing.

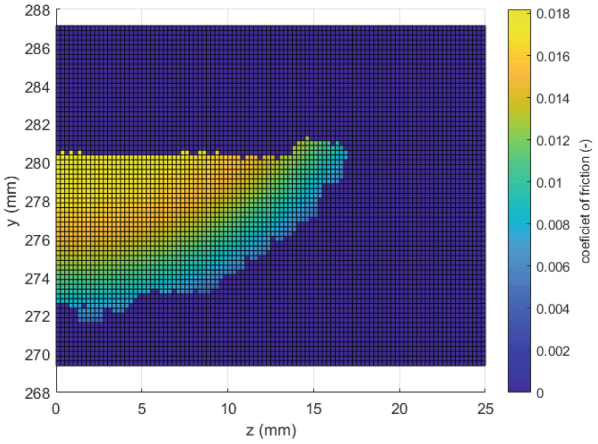

Fig. 12. Distribution of friction coefficient on the contact surface of ring flange of tapered roller bearing.

power loss is generated on the ring flange despite low frictional forces but caused by high slip velocities.

The Fig. 14 shows the dependence of the resulting calculated frictional power loss from the sliding between bearing components (red line). The blue dots represent the measured values of power loss on the test rig, where a pair of tapered roller bearings were measured. Due to the design of the test rig, the friction in the toothed coupling is also included in the measured power loss, therefore the measured values are higher than calculated. However, the calculation of total power loss did not yet include the elastic hysteresis, sliding between the cage and rolling elements and viscous drag of the lubricant because it's very difficult to calculate.

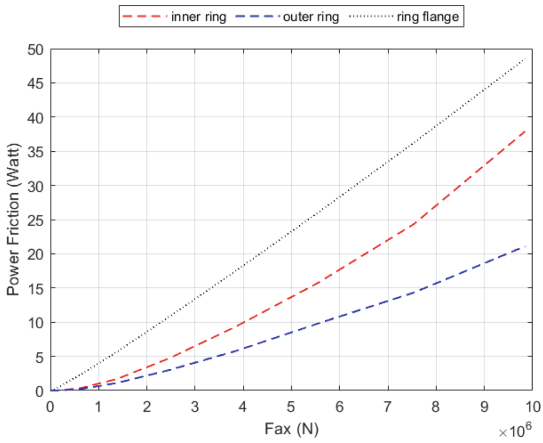

Fig. 13. Partial frictional power loss caused by sliding between frictional surfaces of roller and bearing rings.

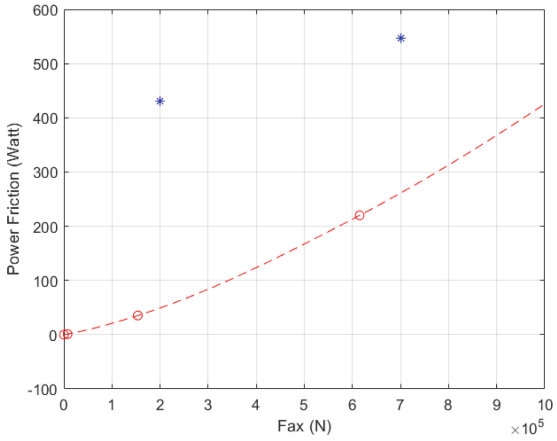

Fig. 14. Overall frictional power loss caused by sliding between bearing components of tapered roller bearing.

4 Conclusions

By the present algorithm it's possible to calculate the frictional power loss between the rolling elements and the raceways and flange of the bearing rings in practically any type of rolling bearing with line contact. Its use is most important for bearings that have a larger nominal contact angle and large differences in orbit radii. Spherical roller bearings are the biggest sufferers [3].

By the proposed algorithm, it is possible to solve the influence of the internal rolling bearing geometry on the resulting frictional power loss, which adversely affect the generate heat and overall efficiency of bearing [5]. The proposed algorithm is an effective

tool in the design process of rolling bearing geometry at early stages of their development. It requires the use of modern software tools, with which frictional power loss can be calculated using the proposed algorithm.

Acknowledgement. This work was supported by Ministry of Education, Science, Research and Sport under the contract No. 1/0595/18 – Optimising the internal geometry of roller bearings with line contact in order to increase their durability and reduce their structural weight.

References

1. Harris, T., A., Kotzalas, M., N.: Advanced Concepts of Bearing Technology. 5th edn. Taylor & Francis Group (2007).
2. Almqvist, A., Wall, P.: Modelling Cavitation in (Elasto)Hydrodynamic Lubrication. Advances in Tribology, Pranav H. Darji, ed, https://www.intechopen.com/books/advances-in-tribology/modelling-cavitation-in-elasto-hydrodynamic-lubrication, (2016).
3. Khonsari, M., M, Booser, E. R.: Applied Tribology, Bearing Design and Lubrication. John Wiley & Sons, INC (2001).
4. Ashby, M. F.: Material Selection in Mechanical Design, 3th edn. Elsevier, Burlington (2005).
5. Madaj, R., Kohar, R.: in the Development of Bearings for Wind Turbines. In: Dynybyl V., Berka, O., Petr, K., Lopot, F., Dub, M. (eds) Latest Methods of Construction Design. 55th International Conference of Machine Design Departments. Prague, Czech Republic. pp 57–62. Springer, Cham (2016).